



# 50-year volume transport of the Soya Warm Current estimated from the sea-level difference and its relationship with the Tsushima and Tsugaru Warm Currents

Kay I. Ohshima<sup>1,2</sup> · Mizuki Kuga<sup>1</sup>

Received: 7 February 2023 / Revised: 3 May 2023 / Accepted: 7 June 2023 / Published online: 22 June 2023  
© The Author(s) 2023

## Abstract

This study provides formulae for monthly estimates of the Soya Warm Current (SYC) transport from the sea-level difference (SLD) across the Soya Strait and along the current, and creates a 50-yr data set of the SYC transport. The formulae are based on the dynamical balance both across the strait and along the current by considering the barotropic and baroclinic components. It is suggested that the barotropic and baroclinic components in transport variability are comparable in summer, whereas the barotropic component is dominant in winter. We compared the 50-year time series of the SYC transport with those of the Tsushima (TSC) and Tsugaru Warm Currents estimated from the SLDs from the viewpoint of the Japan Sea Throughflow (JSTF) system. The variabilities of the SYC and TSC transports are mostly shared for any season, showing relatively high coherence at periods of 2–5 years as well as 1 year. The winter variability of the JSTF transport originates partly from that of the SYC transport caused by the winter monsoon variability in the Sea of Okhotsk. The SYC transport is significantly correlated with the transport through the eastern channel of the TSC, but not that through the western channel. We found difficulty in extracting variability and relationships at periods longer than 5 years among the three transports estimated from the SLDs, probably due to incomplete correction of the ground movements for the sea-level data.

**Keywords** Soya Warm Current · Volume transport · Sea-level difference · Japan Sea throughflow · Geostrophic current

## 1 Introduction

The Japan Sea Throughflow (JSTF) constitutes the inflow through the Tsushima/Korea Strait as the Tsushima Warm Current (TSC), and the outflows through the Tsugaru Strait as the Tsugaru Warm Current (TGC) and the Soya/LaPerouse Strait (hereafter referred to as the Soya Strait) as the Soya Warm Current (SYC) (Fig. 1). The JSTF is driven by the sea-level difference (SLD) between the inflow and outflow ports, which originates from the SLD occurring along the western boundary currents of the Pacific (Minato and Kimura 1980; Toba et al. 1982; Ohshima 1994; Lyu and Kim 2005). On the other hand, the seasonal cycle of the JSTF has

been suggested to be caused by seasonal change in the winds in the Sea of Okhotsk (Tsujino et al. 2008; Kida et al. 2016).

Since the 1990s, the TSC transport has been estimated by many investigations, mainly using an acoustic Doppler current profiler (ADCP) mounted or towed on a ship (Isobe et al. 2002; Teague et al. 2002; Takikawa et al. 2005; Na et al. 2009; Ostrovskii et al. 2009; Fukudome et al. 2010). According to these investigations, the annual average transport lies in the range of 2.4–2.7 Sv (1 Sv =  $10^6 \text{ m}^3 \text{ s}^{-1}$ ). The transport exhibits distinct seasonal variations with an amplitude of 1.1–1.8 Sv, a maximum in October and a minimum in January. The TGC transport has also been investigated using ADCP measurements since the 1990s (Shikama 1994; Ito et al. 2003; Nishida et al. 2003). These observations showed that the annual average transport of the TGC lies in the range of 1.4–1.5 Sv, with a small seasonal amplitude of ~0.3 Sv. Observations by high-frequency ocean radars (referred to as HF radars hereafter) detailed the seasonality of the TSC (Yoshikawa et al. 2010) and the TGC (Kaneko et al. 2021).

✉ Kay I. Ohshima  
ohshima@lowtem.hokudai.ac.jp

<sup>1</sup> Institute of Low Temperature Science, Hokkaido University, Sapporo 060-0819, Japan

<sup>2</sup> Arctic Research Center, Hokkaido University, Sapporo 001-0021, Japan

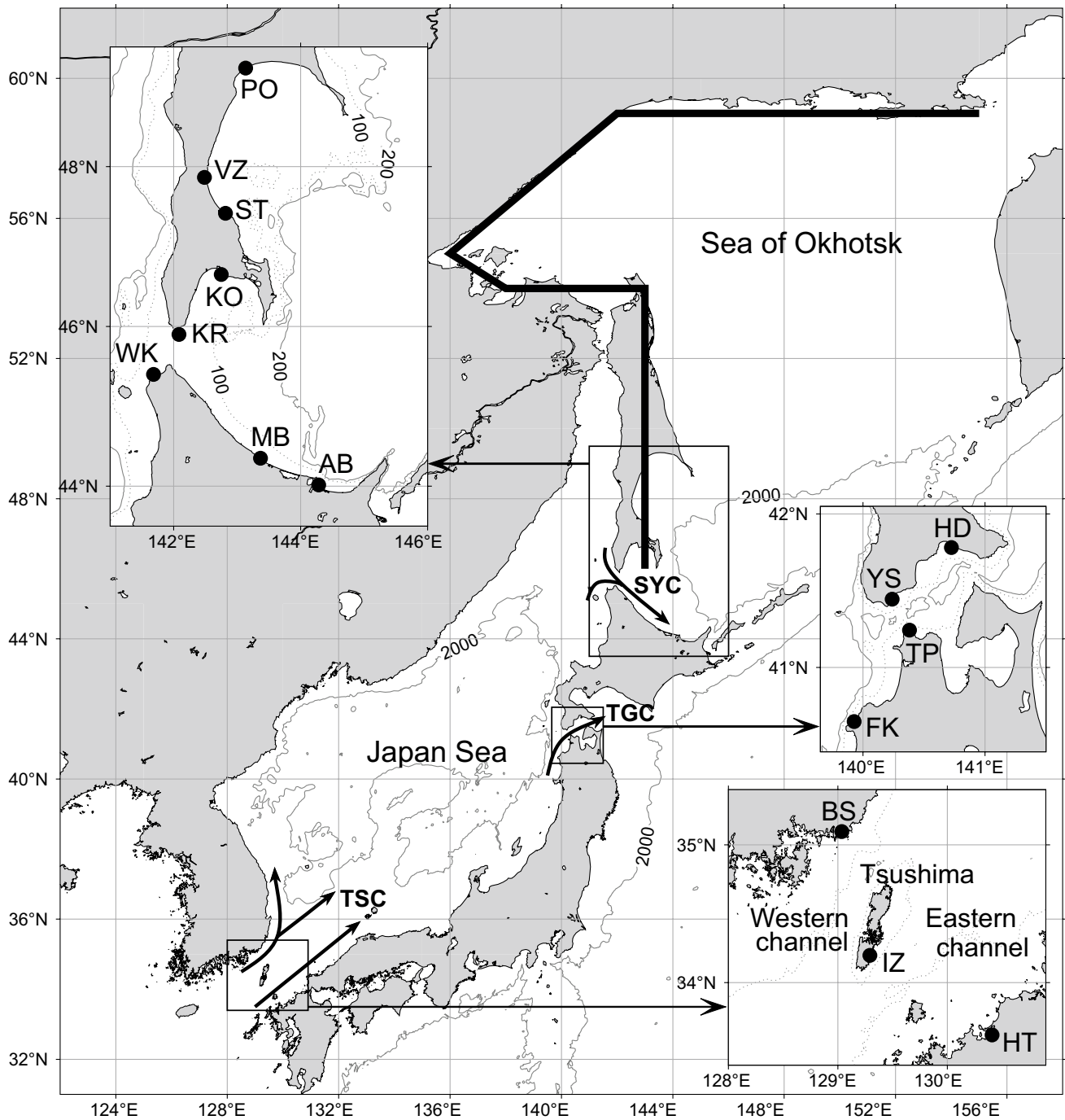


**Fig. 1** A bathymetric map of the straits of the Japan Sea with inset maps of the Soya, Tsugaru, and Tsushima/Korea Straits. The thick arrows indicate the Tsushima, Tsugaru, and Soya Warm Currents, labeled by TSC, TGC, and SYC, respectively. The bathymetry data are derived from the ETOPO1. The bottom contours are 2000 m in

the larger map, 100 m (dotted lines), and 200 m in the inset maps. The locations of the tide gauge stations used in this study are indicated by solid circles with station labels (see Table 1). The thick solid lines along the Okhotsk coast indicate the integration route of the wind stress for calculating the ATW transport from Eq. (1)

Although the SYC transport was estimated only by snapshot observations before the 2000s (e.g., Aota 1975; Tanaka and Nakata 1999; Matsuyama et al. 2006), the surface flow field around the Soya Strait has been continuously monitored by three HF radars since 2003 (Ebuchi

et al. 2006; 2009). Further, Fukamachi et al. (2008) conducted a bottom-mounted ADCP observation near the Soya Strait during 2004–2005 and estimated the annual mean transport of the SYC to be in the range of 0.94–1.04 Sv by combining with the HF radar information. This was the

first quantitative estimation from the direct current measurements. Moreover, Fukamachi et al. (2010) conducted similar observations at the Soya Strait for nearly 2 years during 2006–2008 and estimated the annual mean transport to be 0.8–0.9 Sv. In these estimations, the baroclinic component was not evaluated appropriately because the vertical structure of the current was inferred from only one point of the ADCP. Ohshima et al. (2017) estimated the SYC transport based on measurements using HF radars during 2003–2015 and all available hydrographic data. In their study, the baroclinic velocity structure derived from the climatological geopotential anomaly is combined with the sea surface gradient obtained from radar-derived surface velocities to estimate the absolute velocity structure. According to their estimate, the annual mean transport is 0.91 Sv, with strong seasonal variations, a maximum of 1.41 Sv in August and a minimum of 0.23 Sv in January. According to these estimations of the three currents, the TSC transport is portioned to the TGC transport by 60% and to the SYC transport by 40% in the annual mean, while a major part of the seasonal variation in the TSC transport is shared by that in the SYC transport.

Since the climatological mean and seasonal cycle of the JSTF transport have been clarified by these observations, discussions on interannual variabilities have gained momentum. Kida et al. (2021) showed that the TSC transport has exhibited an increasing trend since the 1990s based on the SLD across the Tsushima/Korea Strait and suggested that this increasing trend is forced by a northward shift in the Kuroshio axis through the propagation of topographic Rossby and Kelvin waves. Shin et al. (2022) proposed that this increasing trend is related to the Pacific decadal oscillation (PDO); the negative PDO causes the weakening of the Kuroshio in the East China Sea and subsequent enhancement of flow toward the Tsushima/Korea Strait. Ohshima et al. (2017) suggested that interannual variations in the SYC transport in winter are partly determined by wind stress along the coast of the Sea of Okhotsk via a mechanism similar to that of the seasonal cycle of the JSTF proposed by Tsujino et al. (2008) and Kida et al. (2016).

To examine the variability of the JSTF transport with up to decadal timescales, long-term estimation of the transport of the three currents is indispensable. For this purpose, the estimation from the SLD provides the longest transport estimation. Regarding the TSC, several studies have proposed formulae to estimate the transport from the SLDs across the strait (Lyu and Kim 2003; Takikawa and Yoon 2005; Nishimura et al. 2008; Shin et al. 2022). Also for the TGC, a formula to estimate the transport was proposed from the SLD across the strait (Nishida et al. 2003). For the SYC, however, the formula was proposed only for the winter season using the SLD along the current (Wakkanai and Abashiri) (see Fig. 1 for the locations). The yearly transport of

the SYC was estimated only for 12 years (2004–2015) when the HF radar data were available (Ohshima et al. 2017).

To date, no observational studies have examined the relationship among the three current transports of the JSTF, because a full set of estimations for the three transports have been provided only in a limited period. The creation of the formula to estimate the SYC transport will provide a full set of long-term estimations of the three current transports, when combined with the estimations from the formulae of the other two current transports. The primary purpose of this study is to develop a formula to estimate the SYC transport from the SLD and to create a 50-yr data set of the SYC transport. For the estimation, we newly used the SLD across the Soya Strait (Wakkanai and Krillion) as well as the SLD along the current (Wakkanai, Monbetsu, and Abashiri). We propose a formula based on the dynamical balance both across the strait and along the current by considering the barotropic and baroclinic components. The second purpose of this study is to examine the relationship between the three current transports of the JSTF, which will provide key suggestions to fully understand the driving and variation mechanisms of the JSTF system.

## 2 Data

We used monthly mean sea-level data mostly provided by the Coastal Movements Data Center (Table 1). All sea levels are barometrically adjusted by atmospheric pressure, with 1 cm corresponding to 1 hPa. Atmospheric pressure data were provided by the Japan Meteorological Agency. If the number of deficit of daily sea-level data is more than 15

**Table 1** Abbreviations and locations of tide gauge stations with the data period used in this study

Station label	Station name	Latitude	Longitude	Data period
PO	Poronaïsk	49°14'N	143°08'E	1965–1988
VZ	Vzmorie	47°52'N	142°29'E	1965–1988
ST	Starodubskoe	47°25'N	142°49'E	1965–1988
KO	Korsakov	46°39'N	142°45'E	1965–1988
KR	Krillion	45°54'N	142°05'E	1965–1988
WK	Wakkanai	45°24'N	141°41'E	1965–2015
AB	Abashiri	44°01'N	144°17'E	1965–2015
MB	Monbetsu	44°21'N	143°22'E	1965–2008
HD	Hakodate	41°47'N	140°43'E	1972–2015
FK	Fukaura	40°39'N	139°56'E	1972–2015
YS	Yoshioka	41°27'N	140°14'E	1984–2002
TP	Tappi	41°15'N	140°23'E	1984–2002
BS	Busan	35°06'N	129°05'E	1965–2015
IZ	Izuhara	34°12'N	129°18'E	1965–2015
HT	Hakata	33°37'N	130°24'E	1967–2015

in a month, that monthly data is regarded as a deficit. The locations of the tide gauge stations are shown in Table 1 and Fig. 1.

In this study, we used wind data in the Sea of Okhotsk to examine the cause of the SLD and to eliminate irregular sea-level data, as described below. The SLD through the Soya Strait in winter is largely determined by the setup of the coastal trapped current and sea level along the east Sakhalin coast, driven by the prevailing northerly wind (Ebuchi et al. 2009; Ohshima et al. 2017). As an index of the setup by the wind, we used the volume transport of arrested topographic waves (ATW) (Csanady 1978), which is represented by:

$$V_{ATW} = \int_0^{y_1} \frac{\tau_y}{\rho_w f} dy, \quad (1)$$

where a right-handed coordinate system is used, with the positive  $x$ -axis pointing offshore and the  $y$ -axis lying along the coastline at  $x=0$ ;  $\tau_y$  is the alongshore component of the wind stress;  $\rho_w$  is the density of seawater; and  $f$  is the Coriolis parameter. Equation (1) implies that the alongshore transport at  $y_1$  becomes the sum of all backward Ekman transport to or from the coast. The integration path is indicated by the thick solid lines in Fig. 1. We used the ATW data estimated in Ohshima et al. (2017), in which the monthly averaged ATW transports were calculated from the 6-hourly wind data at 10 m above the sea surface using the European Centre for Medium-Range Weather Forecasts (ECMWF) reanalysis dataset.

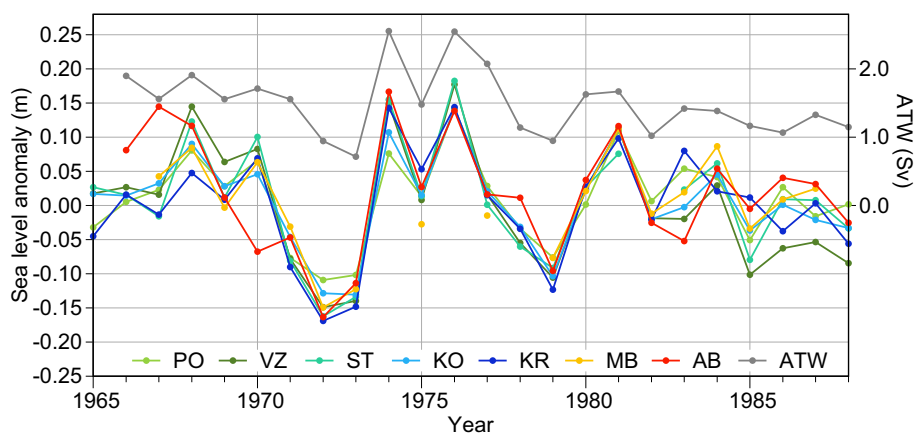
For all the time series of sea-level data, we removed the component fitted to a cubic function from the original sea-level data to correct the ground movement. Regarding the old sea-level data in the Sea of Okhotsk, there seem to be small amounts of irregular data. Such irregular sea-level data at Abashiri and Krillion were removed as follows. In the Sea of Okhotsk, the sea level along the Sakhalin Island and Hokkaido coasts exhibits coherent variations because of the excitation of coastally trapped waves and ATW

by the prevailing northwesterly winds. Figure 2 shows the January sea-level anomalies from the climatological monthly mean at the tide gauge stations in the southern part of the Sea of Okhotsk from 1965 to 1988. It is found that all sea levels show coherent variations corresponding to the ATW (indicated by the gray line). However, the Abashiri data show a few incoherent values, which are regarded as irregular. In this study, if the difference in sea-level anomalies between the Abashiri value and the value averaged over the other five station data exceeded 6 cm, the Abashiri data were regarded as incorrect. In the case of January, data from 1966, 1969, and 1980 were regarded as incorrect. Such data screening was performed in other months and also for the Krillion data. In total, nine data for Abashiri and five for Krillion were regarded as incorrect and eliminated.

### 3 Estimation of the SYC transport from the sea-level difference

In this study, we consider a method that infers the volume transport of the SYC using the SLD across the strait (Wakkanai and Krillion) and along the current (Wakkanai, Monbetsu and Abashiri). For the estimation, we must evaluate the contribution of the barotropic and baroclinic components to the SLD. For this purpose, we used monthly climatological data on barotropic and baroclinic transport of the SYC estimated by Ohshima et al. (2017). We attempted to derive a formulation based on the dynamical balance and the empirical procedure. We assume that the geostrophic relation holds across the strait and that the pressure drop associated with the SLD is balanced by the resistance force (most likely the bottom friction) along the current, which is assumed to be proportional to the current speed or transport.

**Fig. 2** Time series of the January sea-level anomalies from the monthly mean at the tide gauge stations in the southern part of the Sea of Okhotsk for the 24 years, from 1965 to 1988. See Fig. 1 and Table 1 for the locations and station names of the tide gauges, respectively. The ATW transport (gray lines) is also shown, with the scale indicated on the right axis



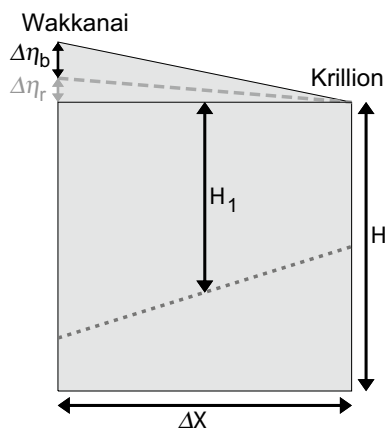


**Fig. 3** Schematics of the conceptual two-layer model.  $\Delta\eta_b$  and  $\Delta\eta_r$  represent the SLDs associated with barotropic and baroclinic velocities, respectively. The baroclinic velocity is defined as the velocity at the upper layer, assuming that the velocity at the lower layer is zero

### 3.1 Dynamical balance across the strait

First, we consider the dynamical balance across the Soya Strait between Wakkanai and Krillion. We consider a two-layer water system with a constant water depth of  $H$  to represent both the barotropic and baroclinic components in the simplest way (Fig. 3). The undisturbed upper layer thickness is set to  $H_1$  and defined as the effective baroclinic depth. The geostrophic current caused by the inclination of the interface of the two layers is derived by assuming that the lower layer velocity is zero, and this upper layer velocity is defined as the baroclinic component. This definition of the baroclinic component is consistent with that reported by Ohshima et al. (2017). In Ohshima et al. (2017), geostrophic currents were calculated based on geopotential anomalies, assuming that the geostrophic current at the bottom is zero. These velocities from the geopotential anomalies are then defined as the baroclinic component of the current. Thus, the vertical integral of the baroclinic velocity is non-zero in this definition, as in our two-layer model.

Under the geostrophic relation, the barotropic and baroclinic velocity,  $v_b, v_r$  is represented by

$$v_b = g/f \times \Delta\eta_b / \Delta x, v_r = g/f \times \Delta\eta_r / \Delta x, \tag{2}$$

where  $\Delta x$  is the width of the strait,  $g$  is gravity acceleration ( $9.8 \text{ m s}^{-2}$ ), and  $\Delta\eta_b, \Delta\eta_r$  is the SLD across the strait associated with the barotropic and baroclinic components, respectively. From Eq. (2), the barotropic and baroclinic volume transport  $V_b (= v_b \times H \times \Delta x), V_r (= v_r \times H_1 \times \Delta x)$  become

$$V_b = g/f \times \Delta\eta_b \times H, V_r = g/f \times \Delta\eta_r \times H_1. \tag{3}$$

Then, the total SLD  $\Delta\eta$  is

$$\Delta\eta = \Delta\eta_b + \Delta\eta_r + \eta_0 = f/(gH) \times V_b + f/(gH_1) \times V_r + \eta_0 = a \times V_b + b \times V_r + \eta_0, \tag{4}$$

$$a = f/(gH), b = f/(gH_1),$$

where  $\eta_0$  (unknown) is the difference between the deviations of the reference points at Wakkanai and Krillion from the geoid.

In this study, we regarded the climatological monthly values of  $\Delta\eta, V_b,$  and  $V_r$  as 12 samples and obtained the values of  $a, b, \eta_0,$  using least squares fitting. The values of  $H$  and  $H_1$  were obtained from  $a$  and  $b$ , respectively. Ohshima et al. (2017) provided the monthly values of  $V_b$  and  $V_r$  for a period of 12 full years, from August 2003 to August 2015. In this study, monthly averages of the 12-year data were used as climatological values (Fig. 4a, Table 2). The climatological monthly  $\Delta\eta$  was calculated using monthly data at Krillion, averaged over 24 years (1965–1988), and that at Wakkanai, averaged over 51 years (1965–2015). The Coriolis parameter  $f$  is set to  $1.039 \times 10^{-4} \text{ (s}^{-1}\text{)}$ , corresponding to the value

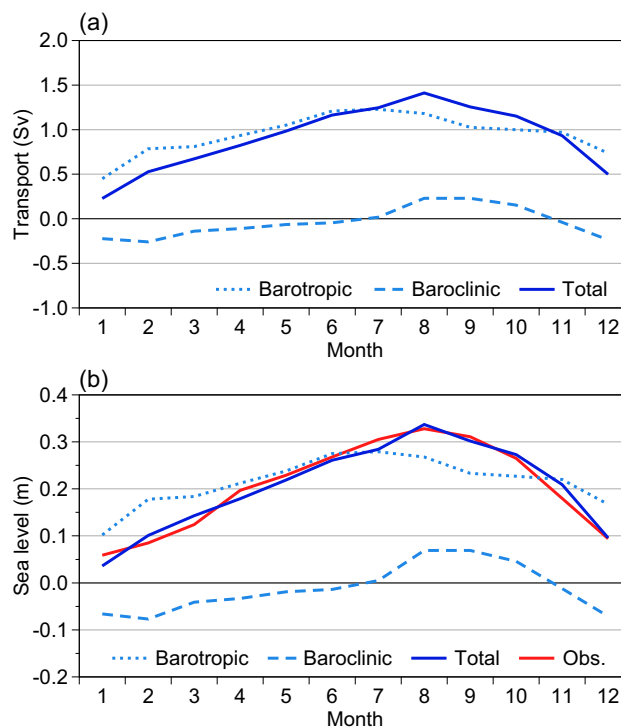


**Fig. 4** **a** Seasonal variations in climatological SYC volume transport estimated in Ohshima et al. (2017). The total SYC transport (solid blue lines), the barotropic component (dotted blue lines), and the baroclinic component (dashed blue lines) are shown. **b** SLD between Wakkanai and Krillion, calculated from the climatological barotropic (dotted blue lines), baroclinic (dashed blue lines), and total (solid blue lines) transports based on Eq. (3). The observed climatology of the SLD between Wakkanai and Krillion is also indicated by the red lines



**Table 2** The monthly and annual volume transports of the SYC estimated in Ohshima et al. (2017)

Month	Total (Sv)	Barotropic (Sv)	Baroclinic (Sv)
1	0.23 ± 0.07	0.45	-0.22
2	0.53 ± 0.13	0.79	-0.26
3	0.67 ± 0.17	0.81	-0.14
4	0.82 ± 0.19	0.93	-0.11
5	0.98 ± 0.17	1.05	-0.07
6	1.16 ± 0.25	1.21	-0.05
7	1.25 ± 0.18	1.23	0.02
8	1.41 ± 0.22	1.18	0.23
9	1.26 ± 0.21	1.03	0.23
10	1.15 ± 0.24	1.00	0.15
11	0.93 ± 0.21	0.97	-0.04
12	0.50 ± 0.27	0.74	-0.24
Mean	0.91 ± 0.07	0.95	-0.04

The error bounds in the transports are standard deviations for the 12 years from 2003 to 2015. Barotropic (column 3) and baroclinic (column 4) components are also shown

at the midpoint of the Soya Strait. The results of the least squares method yielded  $a = 0.227$  (m/Sv),  $b = 0.299$  (m/Sv),  $\eta_0 = 0.187$  (m), and then  $H = 47$  (m),  $H_1 = 35$  (m). Using these values and the values of  $V_b$  and  $V_r$  from Table 2, we obtained the SLDs across the strait from Eq. (4) and compared them with the observed SLDs (Fig. 4b). The agreement is quite good (the Pearson (ordinary) correlation coefficient,  $R$ , is 0.98 and the Spearman correlation coefficient,  $R^*$ , is 0.98). This supports our dynamical setting and the formulation of Eq. (4).

Based on Eq. (4), we consider a method that estimates the monthly SYC transport from the monthly SLD between Wakkanai and Krillion for each year. For a certain month of a certain year, we define the anomalies from the monthly climatological means as  $\delta\eta$ ,  $\delta\eta_b$ ,  $\delta\eta_r$ ,  $\delta V_b$ , and  $\delta V_r$ . Then, the following equation holds from Eq. (4):

$$\delta\eta = \delta\eta_b + \delta\eta_r = (f/gH) \times \delta V_b + (f/gH_1) \times \delta V_r \quad (5)$$

The key issue is how the deviated portion of  $\delta\eta$  is distributed to the barotropic and baroclinic components  $\delta\eta_b$  and  $\delta\eta_r$ . This cannot be determined only by the dynamical balance across the strait.

### 3.2 Dynamical balance along the current

Next, we consider the dynamical balance along the current. In the numerical model (Ohshima and Wakatsuchi 1990) in which the SYC is well reproduced, the SYC is trapped over a relatively shallow slope along the coast and dissipated mainly by bottom friction. Then a sea-level drop occurs

efficiently near the coast. The drop in sea level reflects the dynamical balance between the pressure gradient along the flow and the bottom friction in the model. When the water column is well mixed and homogeneous over the shelf, the coastal flow is considered to be dissipated mainly by the spin down effect associated with the bottom Ekman layer (Brink and Allen 1978). In such a case, bottom friction should be taken to be proportional to the barotropic (bottom) velocity (e.g., Csanady 1978). Based on these studies, we assume that the pressure gradient along the current,  $\Delta\eta_a/\Delta y$ , is balanced by the resistance force associated with the bottom velocity,  $v_{bm}$ . Then, the dynamical balance along the current is likely represented by

$$\Delta\eta_a/\Delta y = C_1 \times v_{bm}, \quad (6)$$

where  $C_1$  is a linear coefficient. In our definition of barotropic velocity (baroclinic velocity is assumed to be zero at the bottom), the bottom velocity  $v_{bm}$  should be proportional to the barotropic transport  $V_b$ .

$$\Delta\eta_a/\Delta y = C_2 \times V_b, \quad (7)$$

where  $C_2$  is a linear coefficient. In strong stratification season, however, the buoyancy shutdown mechanism would work in the bottom layer of the SYC (Karaki et al. 2018), which will be discussed later in Sect. 6.

We examine the relationship of Eq. (7), using the monthly climatological values of the SYC barotropic transport (Table 2) and sea level at Wakkanai, Monbetsu, and Abashiri. When these monthly climatological values are regarded as 12 samples, the barotropic transport has a high correlation with the SLD of Wakkanai–Monbetsu ( $R = 0.92$ ;  $R^* = 0.86$ ) and the SLD of Wakkanai–Abashiri ( $R = 0.92$ ;  $R^* = 0.94$ ). Assuming a linear relationship, the offsets of sea levels between tide gauge stations can be obtained from the intercept of the regression line (zero transport). The absolute sea-level drop can then be obtained by removing these offsets. Figure 5a shows the monthly variation of such sea-level drops at Monbetsu and Abashiri from Wakkanai. Figure 5b shows the scatter plot of the sea-level drops at Monbetsu from Wakkanai versus those at Abashiri, demonstrating a good linear relationship with  $R = 0.99$  and  $R^* = 0.94$ . The relationship between them implies that the sea-level drop at Monbetsu occurs exactly by two-thirds of that at Abashiri. The distance between Monbetsu and Wakkanai is also approximately two-thirds of that between Abashiri and Wakkanai. Figure 5c shows the scatter plot of the SYC barotropic transport versus the absolute sea-level drop at Abashiri, confirming a relatively good linear relationship. These results support Eq. (7): the sea-level drop  $\Delta\eta$  is proportional to the SYC barotropic transport  $V_b$  and alongshore distance  $\Delta y$ .

Assuming that the geostrophic relation (both in barotropic and baroclinic components) is satisfied in the cross-shore

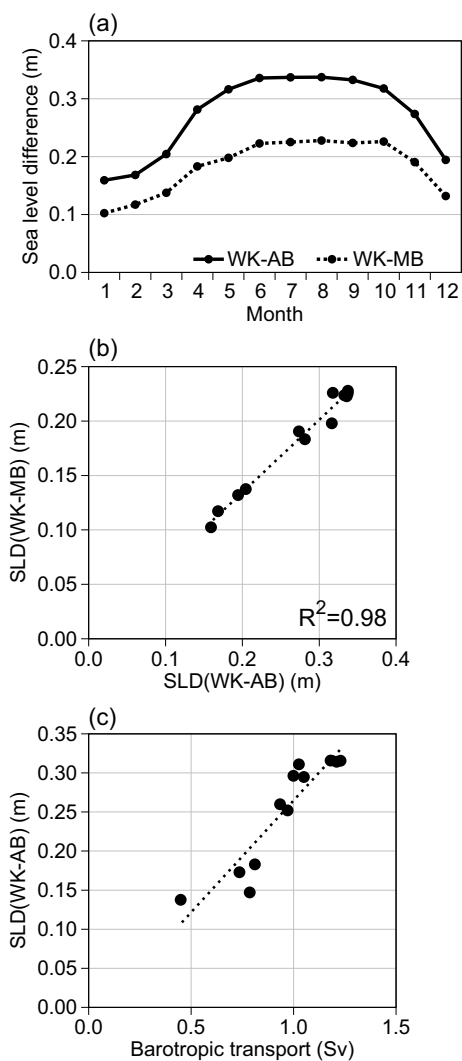


**Fig. 5** **a** Monthly variations in the absolute SLD from Wakkanai to Abashiri (solid lines) and to Monbetsu (dotted lines). **b** Scatter plot of the absolute SLDs from Wakkanai to Abashiri versus those from Wakkanai to Monbetsu for the 12-month samples. **c** Scatter plot of the barotropic SYC transport versus the absolute SLDs from Wakkanai to Abashiri for the 12-month samples. In **b** and **c**, the regression line is indicated by the dotted line

direction in the strait and that the sea-level drop is balanced by the resistance force which is proportional to the bottom or barotropic velocity in the alongshore direction, the variability and relationship between the SLD in the cross-strait and alongshore direction should include information on the ratio of anomalies of baroclinic to barotropic transports. Such a discussion is presented in the following section.

### 3.3 Formulae for estimation of the SYC transport

To estimate the SYC transport from the SLDs, we consider the dynamical balance for the deviation from the

climatological monthly mean. Given anomalies from the climatological monthly mean in SLD between Wakkanai and Krillion,  $\delta\eta_{WK-KR}$ , SLD between Wakkanai and Abashiri,  $\delta\eta_{WK-AB}$ , and anomalies in barotropic and baroclinic transports,  $\delta V_b$ ,  $\delta V_r$ , the following relationships are satisfied by the dynamical balances described in the previous subsection:

$$\delta\eta_{WK-KR} = a \times \delta V_b + b \times \delta V_r, \tag{8}$$

$$\delta\eta_{WK-AB} = d \times \delta V_b. \tag{9}$$

Equation (8) is the balance across the strait derived from Eq. (4), and Eq. (9) is the balance along the current, derived from Eq. (7). The regression analysis between the barotropic transport and the sea-level drop from 12 samples of monthly climatology (Fig. 5c) provides  $d=0.29$  (m/Sv).

Equation (8) divided by Eq. (9) yields:

$$\delta\eta_{WK-KR}/\delta\eta_{WK-AB} = a/d + b/d \times \delta V_r/\delta V_b = \alpha(t) \tag{10}$$

Equation (10) implies that the ratio of the baroclinic to barotropic transport anomalies,  $\delta V_r/\delta V_b$ , is linearly related to  $\delta\eta_{WK-KR}/\delta\eta_{WK-AB}$ . In this study,  $\delta\eta_{WK-KR}/\delta\eta_{WK-AB}$  is assumed to be a function of the month as  $\alpha(t)$  and will be determined later based on the observation. Then, the ratio of the baroclinic to barotropic transport anomalies,  $\delta V_r/\delta V_b$ , is also a function of the month and is represented as

$$\delta V_r/\delta V_b = d\alpha(t)/b - a/b = \beta(t). \tag{11}$$

From Eqs. (9 and 11), the total transport anomaly  $\delta V_t$  ( $=\delta V_b + \delta V_r$ ) is given as

$$\delta V_t = \gamma_1(t) \times \delta\eta_{WK-AB}, \tag{12}$$

$$\gamma_1(t) = \{b + d\alpha(t) - a\}/(bd).$$

Substitution of Eq. (10) into Eq. (12) yields

$$\delta V_t = \gamma_2(t) \times \delta\eta_{WK-KR}, \tag{13}$$

$$\gamma_2(t) = \{b + d\alpha(t) - a\}/\{bd\alpha(t)\}.$$

Equations (12 and 13) provide the empirical formulae of the total transport estimated from the SLD between Wakkanai and Abashiri and between Wakkanai and Krillion, respectively.

On the right-hand side of Eqs. (12 and 13), the values of  $a$ ,  $b$ , and  $d$  have already been obtained as constant values, while the values of  $\alpha(t)$ , which depend on the season, must be determined from the observations. To obtain the values of  $\alpha(t)$  from 24-year (1965–1988) pairs of tide gauge observations, we examine the relation of the observed anomalies calculated by the removal of the climatological monthly mean between Wakkanai–Krillion difference,  $\delta\eta_{WK-KR}$ , and Wakkanai–Abashiri difference,  $\delta\eta_{WK-AB}$ . For all 12 months except

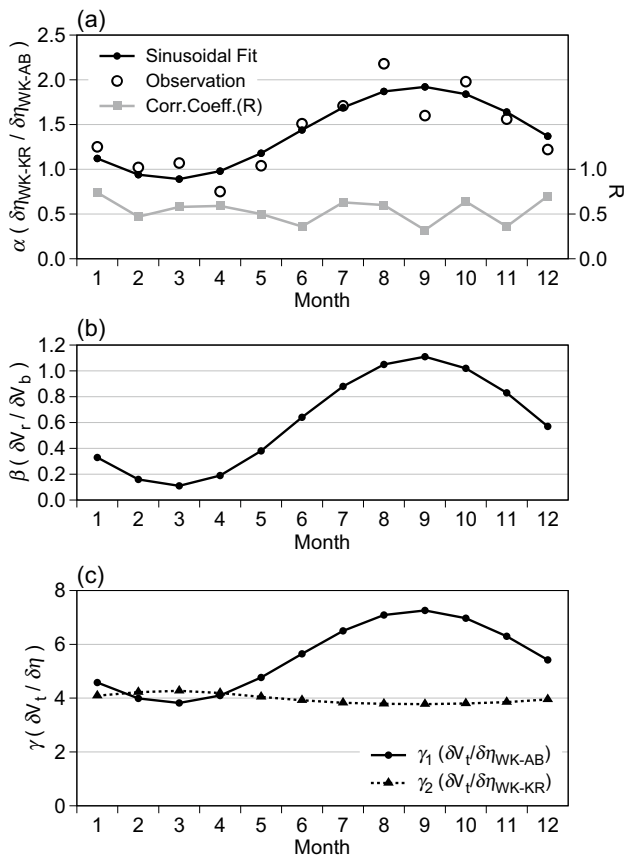


**Fig. 6** **a** Monthly values of the ratio of anomalies in SLD between Wakkanai and Krillion ( $\delta\eta_{WK-KR}$ ) to those between Wakkanai and Abashiri ( $\delta\eta_{WK-AB}$ ) with their correlation coefficients (gray squares and lines). The observed monthly values (open circles) are fitted to a sinusoidal function of 1-year period (solid lines and black circles). These fitted values of  $\alpha(t)$  are used in the empirical formulae (12) and (13). **b** Monthly values of the ratio of the baroclinic transport anomaly to the barotropic transport anomaly [ $\delta V_t/\delta V_b$  ( $=\beta(t)$ )], derived from the fitted values of  $\alpha(t)$ . **c** Monthly values of the ratio of the transport anomaly to the SLD anomaly. The monthly values of  $\gamma_1(t)$  ( $=\delta V_t/\delta\eta_{WK-AB}$ ) are used for the formula using the SLD of Wakkanai–Abashiri, and those of  $\gamma_2(t)$  ( $=\delta V_t/\delta\eta_{WK-KR}$ ) for the formula using the SLD of Wakkanai–Krillion

September, a significant correlation can be obtained between them with a confidence level exceeding 90% (gray squares and lines in Fig. 6a). The inclination obtained from the first principal component for the plots of  $\delta\eta_{WK-KR}$  and  $\delta\eta_{WK-AB}$

for each month is indicated by open circles in Fig. 6a. The obtained values of the inclination ( $=\delta\eta_{WK-KR}/\delta\eta_{WK-AB}$ ) show a clear seasonal variation, with high values in the strong stratification and surface-intensified flow season and low values in the weak stratification and/or bottom-intensified flow season. Instead of using these values of 12 months as  $\alpha(t)$ , we made a sinusoidal fitting (black circles and lines) to the monthly inclination values with 1-year period, and used the fitted values as  $\alpha(t)$  (listed in Table 3) in the empirical formulae.

Now, the total volume transport of the SYC is inferred from Eq. (12) using the SLD anomaly of Wakkanai–Abashiri and from Eq. (13) using the SLD anomaly of Wakkanai–Krillion. The monthly values of  $\alpha(t)$ ,  $\beta(t)$ ,  $\gamma_1(t)$ , and  $\gamma_2(t)$  are presented in Table 3. Once the values of  $\alpha(t)$  are determined, the ratio of the baroclinic to barotropic transport anomalies  $\delta V_t/\delta V_b$  ( $=\beta(t)$ ) can also be obtained (Eq. 11). The seasonal variation of  $\delta V_t/\delta V_b$  (Fig. 6b) shows that the baroclinic component is comparable to the barotropic component from summer to fall when the stratification is strong, while it is much smaller than the barotropic component from winter to spring when the stratification is weak. This is reasonable because stronger stratification can create a larger baroclinic current from the geostrophic relation.

We show the time series of the SYC transports derived from the empirical formulae, using the SLD from Wakkanai to Abashiri and Krillion for 51 years, from 1965 to 2015 (Fig. 7a; Supplemental Tables S1 and S2). It is found that the two transports estimated from the SLD of Wakkanai–Krillion and Wakkanai–Abashiri are in good agreement. Anomalies calculated by removing the climatological monthly mean and their 13-month running mean are also shown in Fig. 7b and c, respectively. There seems to be decadal and subdecadal variability in the SYC transport. These variabilities are discussed later by comparing them with those of the TSC and TGC transports in Sect. 4. In Fig. 7, the transport estimated from the HF radar and hydrographic observations (Ohshima et al. 2017; Supplemental Table S3) is also shown. Although the shorter-timescale variability is in rough agreement between the observation and the estimation from the SLD, a decreasing trend after 2010 only occurs in the observation. We have not yet clarified this disagreement regarding whether the problem lies in the SLD observation or HF

**Table 3** The monthly values of  $\alpha(t)$ ,  $\beta(t)$ ,  $\gamma_1(t)$ , and  $\gamma_2(t)$  used in the formulae for estimating the SYC transport

Month	1	2	3	4	5	6	7	8	9	10	11	12
$\alpha(t)$ $\delta\eta_{WK-KR}/\delta\eta_{WK-AB}$	1.12	0.94	0.89	0.98	1.18	1.44	1.69	1.87	1.92	1.84	1.64	1.37
$\beta(t)$ $\delta V_t/\delta V_b$	0.33	0.16	0.11	0.19	0.38	0.64	0.88	1.05	1.11	1.02	0.83	0.57
$\gamma_1(t)$ $\delta V_t/\delta\eta_{WK-AB}$	4.58	3.99	3.82	4.10	4.77	5.65	6.50	7.09	7.26	6.97	6.30	5.42
$\gamma_2(t)$ $\delta V_t/\delta\eta_{WK-KR}$	4.09	4.22	4.27	4.19	4.05	3.92	3.83	3.79	3.78	3.80	3.85	3.95

$$\alpha(t) = \delta\eta_{WK-KR}/\delta\eta_{WK-AB}, \beta(t) = \delta V_t/\delta V_b = d\alpha(t)/b - a/b, \gamma_1(t) = \delta V_t/\delta\eta_{WK-AB} = \{(b + d\alpha(t) - a)/(bd)\}, \gamma_2(t) = \delta V_t/\delta\eta_{WK-KR} = \{b + d\alpha(t) - a\}/\{bd\alpha(t)\}, a = f/(g H), b = f/(g H_1), d = \delta\eta_{WK-AB}/\delta V_b$$



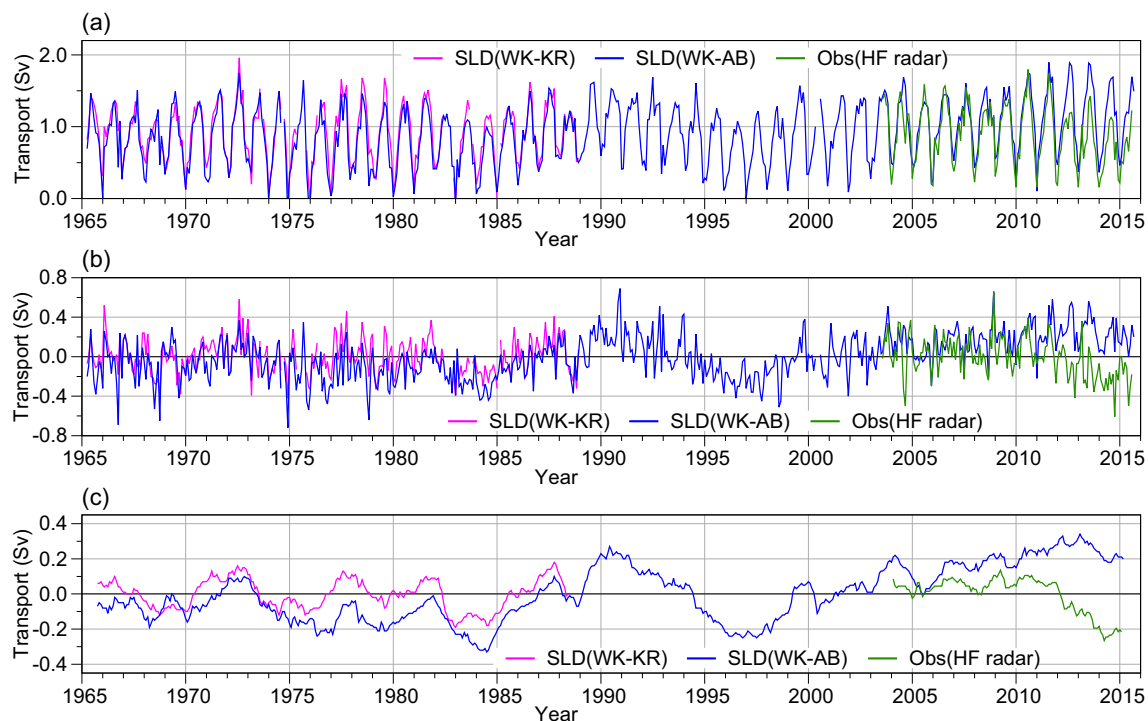


**Fig. 7** The time series of monthly SYC transports estimated based on the empirical formulae from the SLD of Wakkanai–Krillion (purple lines) and the SLD of Wakkanai–Abashiri (navy blue lines) for 51 years from 1965 to 2015, with the transport estimated from HF

radar and hydrographic observations by Ohshima et al. (2017) (green lines). **a** Raw data, including seasonal variations. **b** Anomalies calculated by removing the climatological monthly mean. **c** The 13-month running mean of the anomaly data shown in **b**

observation. The ground movement related to the Great East Japan Earthquake in March 2011 might have affected the sea-level change. To examine the long-term variability of the transport from the SLD, more sophisticated correction of the ground movements for the sea-level data rather than the correction by the fitted cubic function will be needed.

#### 4 Relationship among the three current transports

Given a 50-year time series of the volume transport of the SYC, we compared it with that of the TSC and TGC transports from the viewpoint of the Japan Sea Throughflow (JSTF) system. To infer the long-term variations in the TSC and TGC transports, the SLD across the straits should be used with the geostrophic relationship, as in the case of the SYC transport estimated in this study. Regarding the TSC transport, there have been several empirical formulae to estimate from the SLD (Takikawa and Yoon 2005; Nishimura et al. 2008; Shin et al. 2022), using sea-level data from Hakata, Izuhara, and Busan (see Fig. 1 for the locations). For the TGC, Nishida et al. (2003) proposed a formula for transport from the SLD between Fukaura and Hakodate, and Rikiishi et al. (1989) examined the dynamical balance using

the SLD between Tappi and Yoshioka (see Fig. 1 for the locations).

Before using these formulae, we examined the correlation among all the monthly SLDs across the straits to select the best combination. As pairs of tide gauge stations, we selected Hakata–Busan for the whole Tsushima/Korea Strait, Izuhara–Busan for the western channel of the Tsushima/Korea Strait, Hakata–Izuhara for the eastern channel, Fukaura–Hakodate, Tappi–Yoshioka for the Tsugaru Strait, and Wakkanai–Krillion, Wakkanai–Abashiri for the Soya Strait. The correlations are calculated for the raw data and anomalies from the monthly climatological means (Table 4).

The inflow of the TSC transport should be linked to the outflow of the SYC and/or TGC transports as the JSTF. The SLD of Hakata–Busan, as an index of the total TSC transport, shows a relatively high correlation with both the SLD of Wakkanai–Krillion ( $R=0.75$ ) and Wakkanai–Abashiri ( $R=0.72$ ). This supports the idea that the alongshore SLD can also be used as an index of the SYC transport as well as the cross SLD, as also rationalized in the previous section. The SLD of Hakata–Busan has relatively high correlation with the SLD of Fukaura–Hakodate ( $R=0.82$ ), but it is not highly correlated with the SLD of Tappi–Yoshioka ( $R=0.62$ ). In addition, the data period of Fukaura–Hakodate is much longer than that of Tappi–Yoshioka (Table 1).

**Table 4** Correlations among all SLDs across the Soya, Tsushima/Korea, and Tsugaru Straits, using monthly data from pairs of tide gauge stations

	WK–KR	WK–AB	HT–BS	IZ–BS	HT–IZ	FK–HD	TP–YS
WK–KR	×	0.92	0.75	0.67	0.47	0.67	0.31*
WK–AB	0.72	×	0.72	0.56	0.53	0.62	0.37
HT–BS	0.46	0.42	×	—	—	0.82	0.61
IZ–BS	0.32	0.01*	—	×	—	0.77	0.62
HT–IZ	0.29	0.51	—	—	×	0.39	0.24
FK–HD	0.34	0.18	0.49	0.34	0.29	×	0.70
TP–YS	0.50	0.20+	0.41	0.38	0.21+	0.54	×

Abbreviations of station names are listed in Table 1. The correlations are calculated for the raw data (upper triangle) and anomalies from the monthly climatological mean (lower triangle). Correlation coefficient values not reaching a confidence level of 99.9% and 99% are indicated by cross and asterisk, respectively

Thus, we adopted the SLD of Fukaura–Hakodate for the TGC transport using the empirical formula proposed by Nishida et al. (2003). In this study, to examine the relationship between the transports through the western and eastern channels of the Tsushima/Korea Strait and those of the SYC and TGC transports, we calculated the transports through the western and eastern channels of the Tsushima/Korea Strait. We used the SLD of Izuhara–Busan and Hakata–Izuhara for the transport of the western and eastern channel, respectively. Their sum is regarded as the total TSC transport. Compared to the SLD of Hakata–Busan, the SLDs of Izuhara–Busan and Hakata–Izuhara have a lower but still significant correlation with the SLDs of the Soya and Tsugaru Straits.

The formula inferring the TSC transport from the SLD of Hakata, Izuhara and Busan across the strait was first proposed by Takikawa and Yoon (2005) based on a comparison with the ADCP vertical section observations for 5 years. The formula has been improved by Shin et al. (2022), using much longer-term observation. We adopted the formula proposed by Shin et al. (2022), using the monthly SLD. The volume transports for the two channels,  $V_W$  and  $V_E$ , are calculated by multiplying the calculated geostrophic velocity by the cross-sectional areas:

$$V_W = \zeta_W(t) \times g/f_W \times (\Delta\eta_W - \eta_{0W})/\Delta w_W \times S_W, \tag{14}$$

$$V_E = \zeta_E(t) \times g/f_E \times (\Delta\eta_E - \eta_{0E})/\Delta w_E \times S_E, \tag{15}$$

where  $\Delta\eta$  (m) is the SLD across the channel,  $\eta_0$  (m) is the difference in the reference sea level between the two gauge stations,  $\Delta w$ (m) and  $S$  (m<sup>2</sup>) are the width and cross-sectional area of each channel, with the subscript <sub>W</sub> and <sub>E</sub> indicating the western and eastern channel of the Korea/Tsushima Strait.  $\zeta(t)$  is a correction coefficient of the baroclinic component, which is represented by the sinusoidal function of annual and semi-annual periods (the values are given in Table 3 of Shin et al. 2022). Because we removed the component fitted to a cubic function from the original sea-level

data to correct the ground movement, the values of  $\eta_{0W}$  and  $\eta_{0E}$  do not coincide with the values reported by Shin et al. (2022). Thus, we determined the values of  $\eta_{0W}$  and  $\eta_{0E}$  so that the annual mean transport becomes the same as that of Shin et al. (2022), as our data period is almost the same as that of Shin et al. (2022). Specifically, the annual mean transport through the western and eastern channel is set to 1.51 (Sv) and 1.06 (Sv), respectively.

Regarding the TG transport  $V_{TG}$  (Sv), Nishida et al. (2003) proposed the following formula from the monthly SLD of Fukaura–Hakodate,  $\Delta\eta_{TG}$  (m), based on a comparison with the ADCP vertical section observations.

$$V_{TG} = 2.71 \times (\Delta\eta_{TG} - \eta_{0TG}) + 0.933. \tag{16}$$

In Nishida et al. (2003), the annual mean transport of the TGC is estimated to be 1.50 (Sv) using the SLD from 1959 to 1999 (41 years). Because we removed the fitted cubic line component from the original sea-level data to correct the ground movement, we determined the values of  $\eta_{0TG}$  so that the annual mean transport becomes the same as that of Nishida et al. (2003).

The TSC transport should be the sum of the TGC and SYC transports. According to previous estimates of the annual mean transport, the TSC transport ranges mostly 2.5–2.6 Sv. The formulae of Eqs. (14 and 15) by Shin et al. (2022) provide an annual mean transport of 2.57 Sv. These estimations are somewhat larger than the sum of the TGC and SYC annual transports (1.50 + 0.91 = 2.41 Sv). In our comparison study, we adjusted the annual mean TSC transport to be equivalent to the sum of the TGC and SYC annual transports. According to the reanalysis of the ADCP vertical section observations across the Tsushima/Korea Strait (Utsumi 2018), all the previous estimates (Takikawa and Yoon 2005; Fukudome et al. 2010), including recent estimates (Shin et al. 2022), over-estimated the TSC transport by 5–10% because the set of section routes and their bottom depths were not adequately configured in previous studies. Further, according to the

multi-model ensemble estimation of volume transport through the straits of the Japan Sea with data assimilation, the TSC transport estimated in previous studies was likely overestimated (Han et al. 2016). In this paper, we hold the formulae for the SYC transport proposed in this study and the formula for the TGC transport by Nishida et al. (2003), which gives annual transport of 0.91 Sv and 1.50 Sv, respectively. Because of the likely overestimation of the TSC transport, the formulae for the TSC transport by Shin et al. (2022) are adjusted so that the annual transport of the TSC becomes the sum of the annual transport of the SYC and TGC (2.41 Sv). Specifically, we multiply the factor of 0.94 (2.41/2.57: ratio of the sum of the SYC and TGC annual transport to the TSC annual transport) to the original estimate of the TSC transport by Eqs. (14 and 15).

The TSC transport can be inferred from 1967, when the three tide gauge station data can be obtained. The TGC transport can be inferred from 1972 when Fukaura and Hakodate data can be obtained. Since the temporal resolution of our transport estimation is one month, we focus on the variability on seasonal, annual, and longer timescales, although intra-seasonal variability was found to be prominent in the TSC transport (Ostrovskii et al. 2009).

We first examine the seasonal variations of the three current transports derived from these long-term SLDs. The seasonal variations from the monthly climatological means (Fig. 8a) show that the SYC transport exhibits similar variations in amplitude (1.0 Sv) and phase to those of the TSC transport, as was suggested by Ohshima et al. (2017). In contrast, the TGC transport exhibits a much smaller seasonal variation with an amplitude of 0.3 Sv, which was shown by Nishida et al. (2003). In the seasonal variation, the sum of the SYC and TGC transports does not necessarily coincide with the TSC transport, with a typical difference of 0.1–0.2 Sv for each month. This implies that the estimation method is not complete.

Next, we examine the variability of the three transports for each month based on the standard deviation from the climatological mean (Fig. 8b). For the SYC transport, the standard deviation from the observations for 12 years (2003–2015) is also shown, supporting that the standard deviation of the transport from the SLD represents realistic variability to some extent. From Fig. 8b, the TSC and SYC transports show 2–4 times larger variability than the TGC transport does. Figure 8b also suggests that larger variabilities of the TSC and SYC transports occur during July–December. These analyses suggest that the variability of the TSC transport is linked much more with the SYC transport than with the TGC transport.

Then, the time series of the three current transports of the JSTF are presented and compared (Fig. 9a). For the SYC, the transport inferred from the SLD of Wakkanai–Abashiri

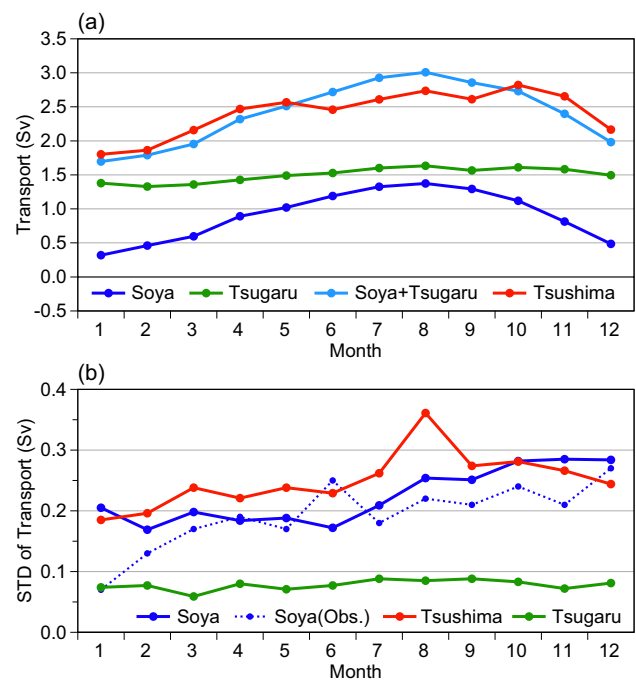


**Fig. 8** The seasonal variations of **a** the volume transport, and **b** its standard deviation from the climatological monthly mean for the SYC (navy blue lines), TSC (red lines), and TGC (green lines), derived from the empirical formulae of the SLDs for the entire analysis period. In **a**, the sum of the SYC and TGC transports is also indicated by the light blue lines. In **b**, the estimation of the SYC transport from observations during 12 years (2003–2015) is shown by navy blue dotted lines

is presented, with the deficit data being substituted by that from the SLD of Wakkanai–Krillion. Figure 9a demonstrates that the TGC transport shows a much smaller variance than the TSC and SYC transports do. A major part of the seasonal variation in the TSC transport is shared by that in the SYC transport.

To raise the sea level in the whole Japan Sea by 1 cm, an inflow of 0.0039 Sv is needed, assuming no outflow. The maximum sea-level change in the Japan Sea in a month is at most 20 cm. This maximum change would occur by the difference of 0.078 Sv between the inflow and outflow, which is an order of magnitude smaller than the typical volume transport of the JSTF, 2.0–3.0 Sv. Therefore, the inflow and outflow should fluctuate nearly coherently in the 1-month resolution (Toba et al. 1982). If the formulae inferring the three transports are exact, the TSC transport should show variations equivalent to those of the sum of the SYC and TGC transports. A comparison of the sum of the SYC and TGC transports with the TSC transport is shown in Fig. 9b. The two transports appear to coincide well with each other, with a correlation coefficient of 0.80. However, this agreement is mostly due to similar seasonal variations. When the seasonal variation is removed using the climatological

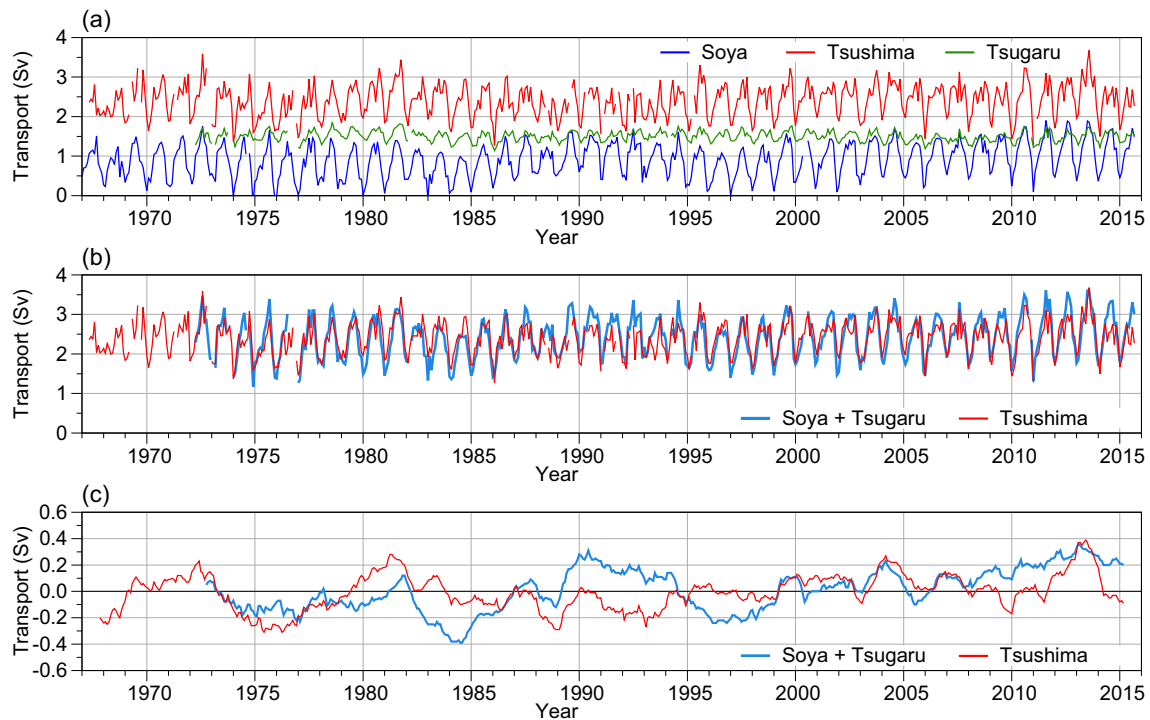


**Fig. 9** Time series of monthly transports of **a** the SYC (navy blue lines), TSC (red lines), and TGC (green lines); **b** the sum of the SYC and TGC (light blue lines) and the TSC (red lines); and **c** their anom-

alies from the climatological monthly mean with the 13-month running mean, estimated based on the empirical formulae from the SLDs for 49 years from 1967 to 2015

monthly mean, the correlation decreases ( $R=0.58$ ), as shown by the 13-month running mean in Fig. 9c. The two transports are in relatively good agreement after the year 2000, while they are not in agreement at all from the 1980s to the 1990s. Each formula has an error, and thus the use of the three formulae should have a larger error.

To examine the variability linkage of the three current transports, we performed a correlation analysis for each month using anomaly data from the monthly climatological means (Fig. 10). The SYC and TGC transports have similar magnitudes of correlation ( $R=0.4\text{--}0.6$ ) with the TSC transport, regardless of the season (Fig. 10a). The sum of the SYC and TGC transports has mostly higher correlation with the TSC transport than the SYC and TGC transports do, implying that the estimation method works to some extent. It is noted that the SYC transport has a significantly high correlation with the transport of the eastern channel of the TSC, but no correlation with that of the western channel for any season (Fig. 10b). This indicates that the SYC transport is mostly linked to the transport of the eastern channel of the TSC. In contrast, the TGC transport has a similar magnitude of correlation ( $R=0.2\text{--}0.5$ ) with that of the eastern and western channels of the TSC, weakly depending on the season (not shown).

To examine the relationships among the three current transports in the frequency domain, we performed spectral

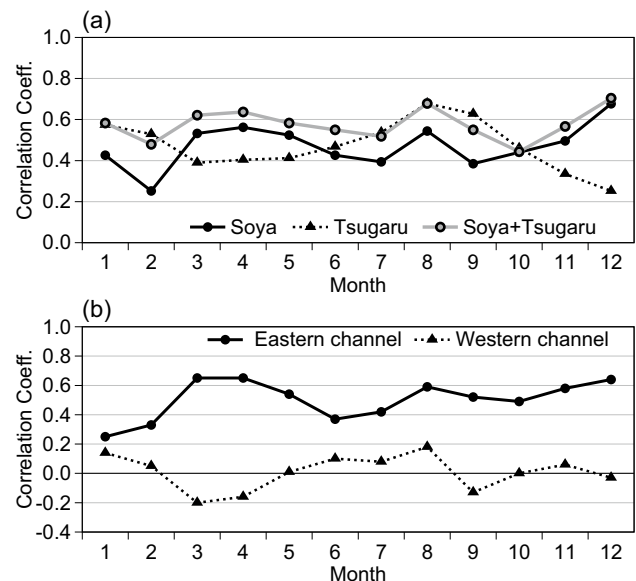


**Fig. 10** Monthly variations in **a** correlation of the TSC transport with the transports of the SYC, TGC, and their sum, and **b** correlation of the SYC transport with the TSC transport in the eastern and western channels

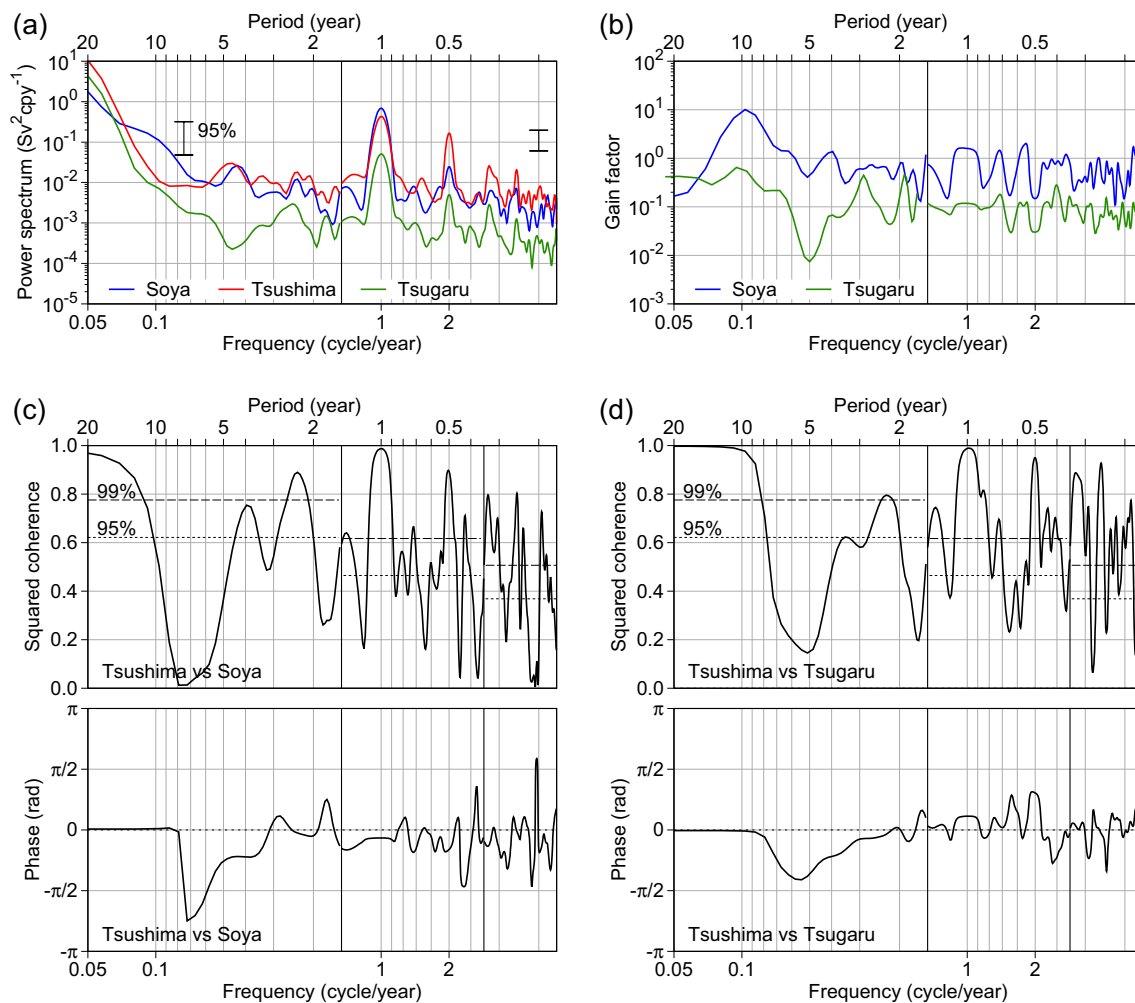


**Fig. 11** **a** Power spectra of the transports of the SYC (blue), TSC (red), and TGC (green). **b** Gain factor of the SYC (blue) and TGC (green) transports to the TSC transport. **c** Squared coherence (upper panel) and phase (lower panel) of the cross-spectra between the TSC and SYC transports. **d** Squared coherence and phase of the cross-

spectra between the TSC and TGC transports. In the lower panel of **c** and **d**, a positive value indicates that the TSC transport leads the SYC or TGC transport. The 95% and 99% confidence intervals are shown in **a**, **c**, and **d**

analysis (Fig. 11). In the power spectra of the TSC and SYC transports (Fig. 11a), a broad peak is identified at periods of 2–5 years, in addition to a strong peak at 1-year period. The gain factor (Fig. 11b) demonstrates that the variability of the TSC transport is mostly shared by that of the SYC transport for a wide range of periods, as well as at 1-year period. From the cross-spectra among the three current transports, the TSC and SYC transports (Fig. 11c) show relatively high coherence at periods of 2–5 years (mostly above the confidence level of 95%) with roughly zero phase shift, where the power spectra of both transports are relatively high (Fig. 11a). At similar periods, a somewhat smaller coherence with roughly zero phase shift is shown between the TSC and TGC transports (Fig. 11d). In contrast, the SYC

and TGC transports does not show high coherence in these periods (less than the 95% confidence level) (not shown).

For longer periods of 5–10 years, the TSC transport does not show significant coherence both with the SYC and TGC transports. In this study, we removed the component fitted to a cubic function from the original sea-level data to correct the ground movement. This procedure would also remove a part of the long-term variability of sea levels. Alternatively, removal of the fitting component cannot completely correct the ground movement. The longer the data period, the larger the accumulated error. If one of the four or five tide gauge stations for the two strait pairs contains incorrect information, the relationship between the two current transports estimated from these station data would not be evaluated appropriately. These problems and the low coherence at periods longer than



5 years suggest the difficulty of extracting long-term variability among the three transports from the SLDs.

## 5 Driving mechanism of the variability of the JSTF transport

Based on numerical model investigations, Tsujino et al. (2008) and Kida et al. (2016) proposed that the seasonal cycle of the JSTF originates from the SYC transport, which is greatly reduced in winter by the setup of the coastal sea level in the Sea of Okhotsk due to the enhanced northerly monsoon. This proposal is consistent with observations from the Sea of Okhotsk. On a seasonal timescale, the coastal branch of the East Sakhalin Current and the associated sea-level setup are driven in winter by the dominant northerly wind along the east coast of Sakhalin and further upstream along the coast (Simizu and Ohshima 2006; Ohshima and Simizu 2008; Nakanowatari and Ohshima 2014). From the dynamic height climatology in the Sea of Okhotsk, the buildup of a positive dynamic height anomaly occurs along the shores from the Sakhalin to Hokkaido coasts during the winter (Mensah et al. 2019). This buildup is associated with the dynamical response of isopycnals to alongshore wind stress, deepening in winter by an enhanced northerly monsoon. In addition, from the satellite altimeters, the sea surface height shows coherent variability trapped over the shelves all along the Okhotsk coast, and their seasonal and interannual variations are strongly correlated with alongshore wind stress, which can be well explained by the ATW (Nakanowatari and Ohshima 2014; Mensah and Ohshima 2020). From these previous studies, the year-to-year variability of the northerly monsoon likely affects the SYC transport and then the JSTF (TSC) transport.

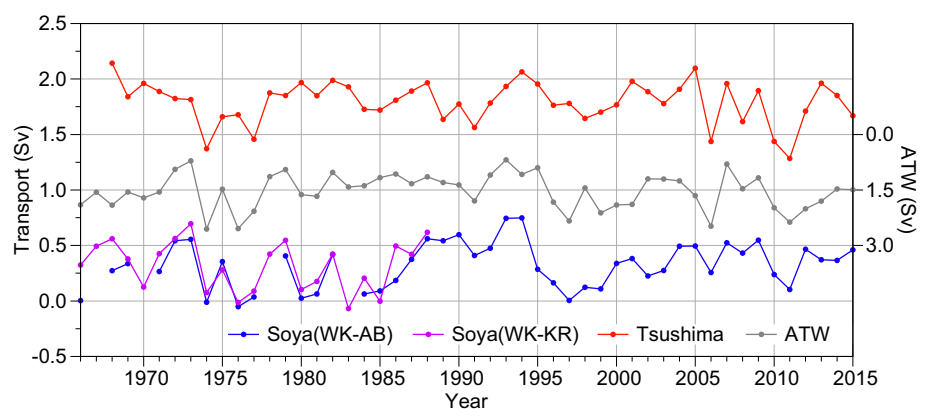
Based on this scenario, we investigated the variability in JSTF transport in winter. As an index of alongshore wind stress along the Okhotsk coast, we used the ATW transport represented by Eq. (1) in Sect. 2. Figure 12 shows the time

series of the SYC transport, the TSC transport, both estimated from the SLDs, and the ATW transport in January for 50 years (1966–2015). The inverted ATW is significantly correlated with the SYC transport ( $R=0.63$ ), as was also shown by Ohshima et al. (2017). Such a correlation can be found in other winter months (Ohshima et al. 2017), but its significance is not high. Additionally, the inverted ATW is significantly correlated with the TSC transport ( $R=0.53$ ). These analyses indicate that the winter variability of the JSTF transport originates partly from that of the SYC transport caused by winter monsoon variability in the Sea of Okhotsk. This is consistent with much larger transport variability of the TSC and SYC than that of the TGC (Figs. 8b and 11a).

In winter, the wind is particularly strong over the coast of the Sea of Okhotsk compared to areas around Japan. This may explain that a part of the winter variability in the JSTF transport originates from the SYC through the change in the SLD at the Soya Strait. There are two types of waves by which the SLD changes propagate from the Soya Strait to the Tsushima/Korea Strait. One is an external gravity or Kelvin wave, and the other is a coastally trapped wave. The coastally trapped wave propagates in an anticlockwise direction around the Japan Sea along the west coast of Sakhalin Island and the Russian coast, which have narrow shelves and thus difficult propagation condition. As suggested by Kida et al. (2016) and Ohshima (1994), information of the SLD change at the Soya Strait should propagate to the Tsushima/Korea Strait through external gravity or Kelvin waves, which have a much larger scale than the strait. Therefore, both western and eastern channels should respond to the SLD changes from the Soya Strait. It should be noted that the correlation of the ATW (wind along the Okhotsk coast) with the SYC/TSC transport is significant, but not very high. The ATW can explain a part of the JSTF variabilities only in winter, but not at all in summer when the wind over the Sea of Okhotsk is weak.

A couple of mechanisms have been proposed that the JSTF variabilities originate from the TSC transport induced

**Fig. 12** Time series of the SYC transport derived from the SLD of Wakkanai–Abashiri (blue lines) and Wakkanai–Krillion (purple lines), the TSC transport (red lines), and the ATW transport (gray lines) in January for 50 years (1966–2015). The scale of the ATW transport is indicated on the right axis and inverted



by the variability of the Kuroshio. Kida et al. (2021) proposed that the north–south shift of the Kuroshio axis affects the sea level along the southern coast of Japan, which propagates to the Tsushima/Korea Strait and then changes the JSTF transport. This mechanism can be well explained by the momentum balance around an island using the island integral constraint (Yang 2007; Kida et al. 2016): a northward shift of the Kuroshio axis enhances the frictional torque by the boundary current, which requires an increase in the frictional torque of the JSTF and thus an increase in its transport. Shin et al. (2022) proposed the strength of the Kuroshio in the East China Sea as the cause of the JSTF transport variability based on a study by Andres et al. (2009). When the Kuroshio is weak, it is topographically controlled because of weakened inertial control. Then, the Kuroshio is steered to the north by topography, and more flow enters the Japan Sea through the Tsushima/Korea Strait. Both mechanisms can explain the increasing trend of the TCS transport from the 1990s to the 2010s because the Kuroshio was weakened and its axis tended to shift northward during that period.

Because the variability of the Kuroshio may occur in any season, it would affect the JSTF variability in any season, which contrasts with the wind variability over the Sea of Okhotsk, which only affects the winter season. The Kuroshio variability affects the JSTF variability, starting from the Tsushima/Korea Strait. This information can propagate to the Soya and Tsugaru Straits with the coast of Japan to the right along a relatively wide shelf via coastally trapped waves within a timescale of less than one month. This may explain the fact that the SYC transport correlates only with the transport of the eastern channel of the Tsushima/Korea Strait for all seasons, and not at all with the western channel transport (Fig. 10b). Larger transport variability of the SYC than that of the TGC (Figs. 8b and 11b) suggests that the disturbances (transport variability) originating from the TSC largely pass through the Tsugaru Strait having narrow width while intrude into the Soya Strait having greater width.

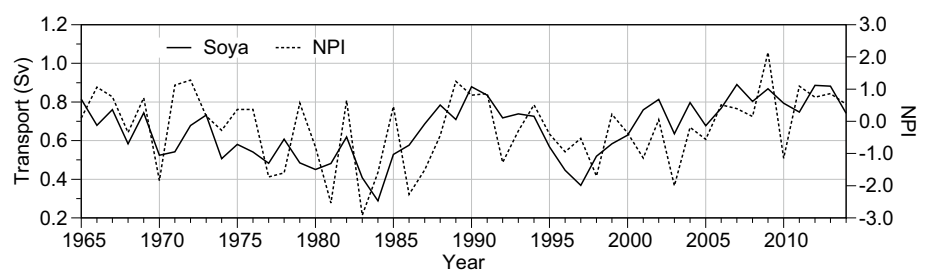
The Japan Sea is the marginal sea adjacent to the western boundary currents in the North Pacific. Thus, the variability of the JSTF (three currents) transport is possibly controlled by the atmospheric circulation variability over the North Pacific. Here, we briefly examine the relationship between the three current transports and atmospheric variability. We

chose the PDO index, the North Pacific Index (NPI), and the Western Pacific pattern as indices of atmospheric variability over the North Pacific and performed a correlation analysis for these indices with the three current transports derived from the SLDs, using yearly mean data. A significant relationship with a confidence level of > 99% was obtained only from the relationship between the NPI and SYC transport ( $R=0.41$ ) and between the PDO index and SYC transport ( $R=0.40$ ). When the period is confined to the winter season (January to May), the correlation between the NPI and SYC transport increased to 0.53. Their time series are shown in Fig. 13. The NPI is an index of Aleutian low strength and is defined as the sea-level pressure averaged over a region from 30–60° N to 160° E–140° W (Trenberth and Hurrell 1994). When the NPI is negative and the Aleutian low is strengthened, the coastal sea level in the Sea of Okhotsk is piled up coherently associated with strengthened ATW (Nakanowatari and Ohshima 2014). Then the SLD between the Japan Sea and the Sea of Okhotsk is reduced, resulting in a significant positive correlation between the NPI and SYC transport. Regarding the TSC and TGC transports, no significant relationship was obtained with any of the three indices. Although the raw yearly mean sea levels at Hakata, Izuhara, and Busan have high negative correlations of  $-0.73$  to  $-0.77$  with the PDO index (Shin et al. 2022), the TSC transport derived from the SLDs was not correlated with the PDO index ( $R=-0.12$ ). These analyses suggest that the variability of the JSTF (three currents) transport is not controlled directly by large-scale atmospheric variability but more likely by local-scale forcing, such as the wind along the Sakhalin coast or the Kuroshio axis near Japan.

## 6 Concluding remarks

This study provides the formulae for monthly estimates of the SYC transport from the SLD of Wakkanai–Krillion across the Soya Strait and that of Wakkanai–Abashiri along the current and creates a 50-yr data set of the SYC transport (Supplemental Tables S1–S3). Since the tide gauge observation at Wakkanai and Abashiri is considered to continue, the SYC transport can be inferred from the formula from now onwards. The formulae are based on the dynamical balance both across

**Fig. 13** Time series of the winter (January to May) SYC transport estimated from the SLD (solid line) and the NPI (dashed line) for 50 years (1965–2014)



the strait and along the current, considering barotropic and baroclinic components. Additionally, analyses of the dynamical balance on the SLDs across and along the current suggest the following findings. 1. The sea-level drop along the current is proportional to barotropic transport (velocity) and along-shore distance. 2. The barotropic and baroclinic components in the transport variability are comparable in summer when the stratification is strong, while the barotropic component is dominant in winter, when the stratification is weak.

In the weak stratification season when the barotropic component is dominant, the sea-level drop is likely balanced by frictional spin down. However, in the strong stratification season when the seasonal thermocline is enhanced, the buoyancy shutdown process would occur owing to the interaction between the seasonal thermocline and the bottom Ekman layer on the coastal slope (Karaki et al. 2018). Then the baroclinic jet associated with the tilting seasonal thermocline is formed with the reduced bottom velocity. In such a case, the buoyancy shutdown suppresses the frictional spin down, which would not be the main balanced force against the sea-level drop. This is consistent with a lower correlation between the sea-level drop and the volume transport in strong stratification season (Ohshima et al. 2017). Even so the alongshore sea-level drop is still correlated with the SLD across the strait (current) to some extent (Fig. 6a), which validates our estimation method. Regarding the dynamical balance along the current during strong stratification season, further discussion will be needed in the future.

Our correlation analyses among the SYC, TGC, and TSC transports estimated from the SLDs suggest the best pairs of tide gauge stations and better formulae for the estimations. Regarding the SYC, both pairs of Wakkanai–Krillion and Wakkanai–Abashiri seem to provide comparably reliable estimations. For the TGC, the formula using the SLD of Fukaura–Hakodate proposed by Nishida et al. (2003) seems to be the best. Regarding the TSC, the most updated formula by Shin et al. (2022) may be the best, as it shows the highest correlation with the SYC and TGC transports among all formulae. However, as pointed out by Utsumi (2018) and Han et al. (2016), their formula tends to overestimate the transport. In this study, we multiplied the factor of 0.94 to their formula to be adjusted to the sum of the SYC and TGC transports (the annual mean of 2.41 Sv).

Using the 50-year time series of the SYC transport derived from the SLDs, we examined the relationships among the three current (JSTF) transports. The variability of the TSC transport is mostly shared by that of the SYC transport for all seasons. The TSC transport shows relatively high coherence with the SYC transport at periods of 2–5 years as well as 1-year period, whereas smaller coherence with the TGC transport. The winter variability of the JSTF transport originates partly from that of the SYC transport caused by the winter monsoon variability in the Sea of

Okhotsk. The SYC transport is significantly correlated with the transport through the eastern channel of the TSC but not with that through the western channel. For longer periods of 5–10 years, the TSC transport does not show significant coherence both with the SYC and TGC transports, probably due to incomplete correction of the ground movements for the sea-level data. This implies the difficulty of the use of the SLDs to extract variability and relationships over longer periods among the three transports.

**Supplementary Information** The online version contains supplementary material available at <https://doi.org/10.1007/s10872-023-00693-6>.

**Acknowledgements** The authors express their gratitude to Kyoko Kitagawa and Vigan Mensah for their support, Naoto Ebuchi and Naoki Hirose for their instructive discussion. Tide gauge data in Japan were provided by Coastal Movements Data Center. Tide gauge data around the Sea of Okhotsk were provided by the Far Eastern Regional Hydro-meteorological Research Institute. Tide gauge data at Busan were provided by Tetsutaro Takikawa and Jong-Hwan Yoon. The figures were produced with the Generic Mapping Tools (GMT) and gnuplot. This work was supported by Grants-in-Aid for Scientific Research (20H05707).

**Data availability** The authors declare that all data supporting the findings of this study are available within the article and its supplementary information file.

**Open Access** This article is licensed under a Creative Commons Attribution 4.0 International License, which permits use, sharing, adaptation, distribution and reproduction in any medium or format, as long as you give appropriate credit to the original author(s) and the source, provide a link to the Creative Commons licence, and indicate if changes were made. The images or other third party material in this article are included in the article's Creative Commons licence, unless indicated otherwise in a credit line to the material. If material is not included in the article's Creative Commons licence and your intended use is not permitted by statutory regulation or exceeds the permitted use, you will need to obtain permission directly from the copyright holder. To view a copy of this licence, visit <http://creativecommons.org/licenses/by/4.0/>.

## References

- Andres M, Park JH, Wimbush M, Zhu XH, Nakamura H, Kim K, Chang K-I (2009) Manifestation of the Pacific decadal oscillation in the Kuroshio. *Geophys Res Lett* 36:L16602. <https://doi.org/10.1029/2009GL039216>
- Aota M (1975) Studies on the Soya Warm Current. *Low Temp Sci* A33:151–172 (**In Japanese with English summary**)
- Brink KH, Allen JS (1978) On the effect of bottom friction on barotropic motion over the continental shelf. *J Phys Oceanogr* 8:919–922
- Csanady GT (1978) The arrested topographic wave. *J Phys Oceanogr* 8:47–62
- Ebuchi N, Fukamachi Y, Ohshima KI, Shirasawa K, Ishikawa M, Takatsuka T, Daibo T, Wakatsuchi M (2006) Observation of the Soya Warm Current using HF ocean radar. *J Oceanogr* 62:47–61
- Ebuchi N, Fukamachi Y, Ohshima KI, Wakatsuchi M (2009) Subinertial and seasonal variations in the Soya Warm Current revealed by HF ocean radars, coastal tide gauges, and bottom-mounted ADCP. *J Oceanogr* 65:31–43

- Fukamachi Y, Tanaka I, Ohshima KI, Ebuchi N, Mizuta G, Yoshida H, Takayanagi S, Wakatsuchi M (2008) Volume transport of the Soya Warm Current revealed by bottom-mounted ADCP and ocean-radar measurement. *J Oceanogr* 64:385–392
- Fukamachi Y, Ohshima KI, Ebuchi N, Bando T, Ono K, Sano M (2010) Volume transport in the Soya Strait during 2006–2008. *J Oceanogr* 66:685–696
- Fukudome K, Yoon J-H, Ostrovskii A, Takikawa T, Han I-S (2010) Seasonal volume transport variation in the Tsushima Warm Current through the Tsushima Straits from 10 years of ADCP observations. *J Oceanogr* 66:539–551. <https://doi.org/10.1007/s10872-010-0045-5>
- Han S, Hirose N, Usui N, Miyazawa Y (2016) Multi-model ensemble estimation of volume transport through the straits of the East/Japan Sea. *Ocean Dyn* 66:59–76. <https://doi.org/10.1007/s10236-015-0896-9>
- Isobe A, Ando M, Watanabe T, Senjyu T, Sugihara S, Manda A (2002) Freshwater and temperature transports through the Tsushima-Korea Straits. *J Geophys Res* 107:3065. <https://doi.org/10.1029/2000JC000702>
- Ito T, Togawa O, Ohnishi M, Isoda Y, Nakayama T, Shima S, Kuroda H, Iwahashi M, Sato C (2003) Variation of velocity and volume transport of the Tsugaru Warm Current in the winter of 1999–2000. *Geophys Res Lett* 30:1678. <https://doi.org/10.1029/2003GL017522>
- Kaneko H, Sasaki K, Abe H, Tanaka T, Wakita M, Watanabe S, Okunishi T, Sato Y, Tatamisashi S (2021) The role of an intense jet in the Tsugaru Strait in the formation of the outflow gyre revealed using high-frequency radar data. *Geophys. Res. Lett.* 48:e2021GL092909. <https://doi.org/10.1029/2021GL092909>
- Karaki T, Mitsudera H, Kuroda H (2018) Buoyancy shutdown process for the development of the baroclinic jet structure of the Soya Warm Current during summer. *J Oceanogr* 74:339–350
- Kida S, Qiu B, Yang J, Lin X (2016) The annual cycle of the Japan Sea Throughflow. *J Phys Oceanogr* 46:23–39. <https://doi.org/10.1175/JPO-D-15-0075.1>
- Kida S, Takayama K, Sasaki Y, Matsuura H, Hirose N (2021) Increasing trend in Japan Sea throughflow transport. *J Oceanogr* 77:145–153. <https://doi.org/10.1007/s10872-020-00563-5>
- Lyu SJ, Kim K (2003) Absolute transport from the sea level difference across the Korea Strait. *Geophys Res Lett* 30:1285. <https://doi.org/10.1029/2002GL016233>
- Lyu SJ, Kim K (2005) Subinertial to interannual transport variations in the Korea Strait and their possible mechanisms. *J Geophys Res* 110:C12016. <https://doi.org/10.1029/2004JC002651>
- Matsuyama M, Wadaka M, Abe T, Aota M, Koike Y (2006) Current structure and volume transport of the Soya Warm Current in summer. *J Oceanogr* 62:197–205
- Mensah V, Ohshima KI (2020) Variabilities of the sea surface height in the Kuril Basin of the Sea of Okhotsk: coherent shelf-trapped mode and Rossby Normal Modes. *J Phys Oceanogr* 50:2289–2313. <https://doi.org/10.1175/JPO-D-19-0216.1>
- Mensah V, Ohshima KI, Nakanowatari T, Riser S (2019) Seasonal changes of water mass, circulation and dynamic response in the Kuril Basin of the Sea of Okhotsk. *Deep-Sea Research Part I* 144:115–131. <https://doi.org/10.1016/j.dsr.2019.01.012>
- Minato S, Kimura R (1980) Volume transport of the western boundary current penetrating into a marginal sea. *J Oceanogr Soc Japan* 36:185–195
- Na H, Isoda Y, Kim K, Kim YH, Lyu SJ (2009) Recent observations in the straits of the East/Japan Sea: a review of hydrography, currents and volume transports. *J Marine Systems* 78:200–205
- Nakanowatari T, Ohshima KI (2014) Coherent sea level variation in and around the Sea of Okhotsk. *Prog Oceanogr* 126:58–70. <https://doi.org/10.1016/j.pocean.2014.05.009>
- Nishimura K, Hirose N, Fukudome K (2008) Long-term estimation of volume transport through the Tsushima Straits, Kushyu Univ. Rep 135:113–118 (In Japanese with English summary)
- Nishida Y, Kanomata I, Tanaka I, Sato S, Takahashi S, Matsubara H (2003) Seasonal and interannual variations of the volume transport through the Tsugaru Strait. *Umi No Kenkyu* 12:487–499 (In Japanese with English abstract)
- Ohshima KI (1994) The flow system in the Japan Sea caused by a sea level difference through shallow straits. *J Geophys Res* 99:9925–9940
- Ohshima KI, Wakatsuchi M (1990) A numerical study of barotropic instability associated with the Soya Warm Current in the Sea of Okhotsk. *J Phys Oceanogr* 20:570–584
- Ohshima KI, Simizu D (2008) Particle tracking experiments on a model of the Okhotsk Sea: toward oil spill simulation. *J Oceanogr* 64:103–114
- Ohshima KI, Simizu D, Ebuchi N, Morishima S, Kashiwase H (2017) Volume, heat, and salt transports through the Soya Strait and their seasonal and interannual variations. *J Phys Oceanogr* 47:999–1019. <https://doi.org/10.1175/JPO-D-16-0210.1>
- Ostrovskii AG, Fukudome K, Yoon JH, Takikawa T (2009) Variability of the volume transport through the Korea/Tsushima Strait as inferred from the shipborne acoustic Doppler current profiler observations in 1997–2007. *Oceanology* 49:338–349
- Rikiishi K, Sato H, Matsuo S (1989) Sea surface inclination due to the effect of the Coriolis force on an ocean current. *J Geophys Res* 94:3237–3246
- Shikama N (1994) Current measurement in the Tsugaru Strait using the bottom-mounted ADCPs. *Kaiyo Monthly* 26:815–818 (In Japanese)
- Shin H-R, Lee J-H, Kim C-H, Yoon J-H, Hirose N, Takikawa T, Cho K (2022) Long-term variation in volume transport of the Tsushima warm current estimated from ADCP current measurement and sea level differences in the Korea/Tsushima Strait. *J. Marine Syst* 232:103750. <https://doi.org/10.1016/j.jmarsys.2022.103750>
- Simizu D, Ohshima KI (2006) A model simulation on the circulation in the Sea of Okhotsk and the East Sakhalin Current. *J Geophys Res* 111:C05016. <https://doi.org/10.1029/2005JC002980>
- Takikawa T, Yoon J-H (2005) Volume transport through the Tsushima Straits estimated from sea level difference. *J Oceanogr* 61:699–708. <https://doi.org/10.1007/s10872-005-0077-4>
- Takikawa T, Yoon J-H, Cho K-D (2005) The Tsushima Warm Current through Tsushima Straits estimated from ferryboat ADCP data. *J Phys Oceanogr* 35:1154–1168
- Tanaka I, Nakata A (1999) Results of direct current measurement in the La Perouse Strait (the Soya Strait), 1995–1998. *PICES Sci Rep* 12:173–176
- Teague WJ, Jacobs GA, Perkins HT, Book JW, Chang K-I, Suk M-S (2002) Low-frequency current observations in the Korea/Tsushima Strait. *J Phys Oceanogr* 32:1621–1641
- Toba Y, Tomizawa K, Kurasawa Y, Hanawa K (1982) Seasonal and year-to-year variability of the Tsushima-Tsugaru Warm Current system with its possible cause. *La Mer* 20:41–51
- Trenberth KE, Hurrell JW (1994) Decadal atmosphere-ocean variations in the Pacific. *Clim Dyn* 9:303–319
- Tsujino H, Nakano H, Motoi T (2008) Mechanism of currents through the straits of the Japan Sea: mean state and seasonal variation. *J Oceanogr* 64:141–161
- Utsumi Y (2018) Reanalysis of the flow field across the Tsushima Strait estimated from ferry boat ADCP data. Master's thesis, Interdisciplinary Graduate School of Engineering Sciences, Kyushu University. (In Japanese)
- Yang J (2007) An oceanic current against the wind: how does Taiwan Island steer warm water into the East China Sea? *J Phys Oceanogr* 37:2563–2569
- Yoshikawa Y, Masuda A, Marubayashi K, Ishibashi M (2010) Seasonal variations of the surface currents in the Tsushima Strait. *J Oceanogr* 66:223–232